



Methane releases  
from Arctic shelves

A. Berchet et al.

This discussion paper is/has been under review for the journal Atmospheric Chemistry and Physics (ACP). Please refer to the corresponding final paper in ACP if available.

# Atmospheric constraints on the methane emissions from the East Siberian Shelf

A. Berchet<sup>1,a</sup>, P. Bousquet<sup>1</sup>, I. Pison<sup>1</sup>, R. Locatelli<sup>1</sup>, F. Chevallier<sup>1</sup>, J.-D. Paris<sup>1</sup>,  
E. J. Dlugokencky<sup>2</sup>, T. Laurila<sup>3</sup>, J. Hatakka<sup>3</sup>, Y. Viisanen<sup>3</sup>, D. E. J. Worthy<sup>4</sup>,  
E. G. Nisbet<sup>5</sup>, R. E. Fisher<sup>5</sup>, J. L. France<sup>5</sup>, D. Lowry<sup>5</sup>, and V. Ivakhov<sup>6</sup>

<sup>1</sup>Laboratoire des Sciences du Climat et de l'Environnement, CEA-CNRS-UVSQ, IPSL, Gif-sur-Yvette, France

<sup>2</sup>NOAA Earth System Research Laboratory, Global Monitoring Division, Boulder, CO, USA

<sup>3</sup>Climate and Global Change Research, Finnish Meteorological Institute, Helsinki, Finland

<sup>4</sup>Environment Canada, Toronto, Ontario, Canada

<sup>5</sup>Department of Earth Sciences, Royal Holloway, University of London, Egham, UK

<sup>6</sup>Voeikov Main Geophysical Observatory, St Petersburg, Russia

<sup>a</sup>now at: Laboratory for Air Pollution/Environmental Technology, Swiss Federal Laboratories for Materials Science and Technology, Empa, Dübendorf, Switzerland

Received: 26 August 2015 – Accepted: 27 August 2015 – Published: 17 September 2015

Correspondence to: A. Berchet (antoine.berchet@empa.ch)

Published by Copernicus Publications on behalf of the European Geosciences Union.

Title Page

Abstract

Introduction

Conclusions

References

Tables

Figures



Back

Close

Full Screen / Esc

Printer-friendly Version

Interactive Discussion



## Abstract

Sub-sea permafrost and hydrates in the East Siberian Arctic Ocean Continental Shelf (ESAS) constitute a substantial carbon pool, and a potentially large source of methane to the atmosphere. Previous studies based on interpolated oceanographic campaigns estimated atmospheric emissions from this area at 8–17 TgCH<sub>4</sub>y<sup>-1</sup>. Here, we propose insights based on atmospheric observations to evaluate these estimates. Isotopic observations suggest a biogenic origin (either terrestrial or marine) of the methane in air masses originating from ESAS during summer 2010. The comparison of high-resolution simulations of atmospheric methane mole fractions to continuous methane observations during the entire year 2012 confirms the high variability and heterogeneity of the methane releases from ESAS. Simulated mole fractions including a 8 TgCH<sub>4</sub>y<sup>-1</sup> source from ESAS are found largely overestimated compared to the observations in winter, whereas summer signals are more consistent with each other. Based on a comprehensive statistical analysis of the observations and of the simulations, annual methane emissions from ESAS are estimated in a range of 0.5–4.3 TgCH<sub>4</sub>y<sup>-1</sup>.

## 1 Introduction

Most long-range global climate projections forecast a warming in the Arctic of at least a few °C over the next decades (Collins et al., 2013). Warmer Arctic temperatures could induce the thawing of continental and submarine permafrost and the destabilization of marine hydrates, causing massive methane emissions into the atmosphere, and hence, generating positive feedbacks to the regional and global warming. Monitoring methane emissions at high latitudes in the North Hemisphere is therefore of critical importance to anticipate and to interpret future climate changes. The different potential sources emitting methane in the Arctic are identified, but the regional methane budget still has significant uncertainties, depending on the method used for its assessment. For example, on the one side, emissions of methane from the Arctic tundra estimated

ACPD

15, 25477–25501, 2015

## Methane releases from Arctic shelves

A. Berchet et al.

Title Page

Abstract

Introduction

Conclusions

References

Tables

Figures

◀

▶

◀

▶

Back

Close

Full Screen / Esc

Printer-friendly Version

Interactive Discussion



## Methane releases from Arctic shelves

A. Berchet et al.

Title Page

Abstract

Introduction

Conclusions

References

Tables

Figures

◀

▶

◀

▶

Back

Close

Full Screen / Esc

Printer-friendly Version

Interactive Discussion



by flux observations and process-based models (i.e. bottom-up approaches) for the 2000s have been synthesized respectively at 20 (11 to 51) Tg CH<sub>4</sub> y<sup>-1</sup> and 28 (18 to 37) Tg CH<sub>4</sub> y<sup>-1</sup> (McGuire et al., 2009). On the other side, top-down atmospheric inversions, based on methane atmospheric observations, show a range for total natural Arctic methane emissions north of 60° N of 16 (12–28) Tg CH<sub>4</sub> y<sup>-1</sup> (Kirschke et al., 2013), i.e. smaller and slightly narrower than the bottom-up range, but still statistically consistent with bottom-up estimates. In addition, anthropogenic emissions are estimated at 9 (7 to 11) Tg CH<sub>4</sub> y<sup>-1</sup> above 60° N by top-down inversions (Kirschke et al., 2013).

Methane emissions from the Arctic Ocean are lower than land emissions, but more uncertain relatively, as synthesized by McGuire et al. (2009), with a range of 1–12 Tg CH<sub>4</sub> y<sup>-1</sup>. The East Siberian Arctic Shelf (ESAS), which covers 2 × 10<sup>6</sup> km<sup>2</sup> or 14 % of the Arctic Ocean, constitutes a large pool of carbone for potential Arctic CH<sub>4</sub> emissions as most of Arctic marine permafrost (possibly up to 80 %; see supplementary material in Shakhova et al., 2010) is located in this region after the flooding of Siberian tundra during the Holocene transgression (7–15 ky ago). Marine hydrates are also a large pool of sub-sea methane, with very uncertain global emissions (2–9 Tg CH<sub>4</sub> y<sup>-1</sup>; Kirschke et al., 2013). Based on oceanographic measurements performed over almost a decade, Shakhova et al. (2010) suggested that ESAS emits 8 Tg CH<sub>4</sub> y<sup>-1</sup> into the Arctic atmosphere, that is 2/3 of the 1–12 Tg CH<sub>4</sub> y<sup>-1</sup> range by McGuire et al. (2009). Shakhova et al. (2014) revised ESAS emissions upwards at 17 Tg CH<sub>4</sub> y<sup>-1</sup>, accounting for methane emissions above several oceanic hotspots due to bubbling in the water-column and methane degassing to the atmosphere during storms.

Observations of atmospheric methane mole fractions and of methane isotopes in the Arctic can improve our understanding of ESAS emissions (Fisher et al., 2011). North of 55° N, 22 atmospheric stations measure methane mole fractions, among which 6 sites provide continuous observations and 3 sites sample the isotopic composition of air on weekly basis or during intensive campaigns. Although sparse, these stations are well illuminated by ocean and land methane emissions because of fast horizontal transport of air masses around the North Pole (e.g., Bousquet et al., 2011, and Supplement).

## Methane releases from Arctic shelves

A. Berchet et al.

Title Page

Abstract

Introduction

Conclusions

References

Tables

Figures



Back

Close

Full Screen / Esc

Printer-friendly Version

Interactive Discussion



In this paper, atmospheric methane observations and high-resolution simulations of atmospheric transport in the Arctic are combined to evaluate the potential of a  $8 \text{ TgCH}_4 \text{ y}^{-1}$  source from ESAS and to propose atmospheric insights on ESAS methane emission magnitude. In Sect. 2, the observations and the transport model set up are described as such as the statistical analysis used to compare simulations to measurements. In Sect. 3.1, Arctic isotopic  $\text{CH}_4$  measurements are analysed to confirm the geophysical origin of ESAS methane emissions. In Sect. 3.2, simulations from a  $8 \text{ TgCH}_4 \text{ y}^{-1}$  reference scenario are compared to observed time series of  $\text{CH}_4$  to assess the likelihood of such a reference scenario. In Sect. 3.3, a comprehensive statistical analysis based on Monte Carlo experiments (described in Sect. 2.4) is carried out to propose a range of ESAS emission magnitudes compatible with circumpolar atmospheric observations.

## 2 Materials and methods

### 2.1 Observation sites

This study is based on the statistical analysis of the synoptic signal. Therefore, we compare meso-scale simulations only to continuous methane measurements. Our analysis of continuous observations is also limited to the year 2012 for data availability reasons. Out of the active observation sites carrying out continuous atmospheric measurements of methane mole fractions around the Arctic Ocean in 2012, we selected 4 sites downwind the ESAS: 1 nearby site, 2 sites remotely but regularly illuminated by ESAS emissions, and 1 background site only poorly influenced by ESAS emissions (Fig. 1). The remaining sites are either barely influenced by ESAS, or local and regional influences are dominant (e.g., Siberian lowlands for observation sites of JR-STATION network; Sasakawa et al., 2010). Tiksi (TIK) is located closest to the shores of the Laptev sea, a few hundreds kilometres away from the core of the emitting region detected by Shakhova et al. (2010, 2014). Barrow (BRW) and Alert (ALT) are located

**Methane releases  
from Arctic shelves**

A. Berchet et al.

Title Page

Abstract

Introduction

Conclusions

References

Tables

Figures



Back

Close

Full Screen / Esc

Printer-friendly Version

Interactive Discussion



at the northern edge of North America, in north Alaska and north Canada respectively, about 2000–2500 km away from the ESAS but still influenced by this region (see Figs. S7, S8 and 4). Air masses originating from ESAS are most of the time transported to the observation sites directly across the Arctic ocean in 2–3 days. Therefore, usually no major continental emission areas lie along the air mass paths from ESAS to BRW or ALT stations. Pallas (PAL), in northern Scandinavia, is taken as a distant site, with dominant influence from Europe (see Fig. S9) and very limited influence by Laptev Sea emissions (typical contributions < 2 ppb; maximum 20 ppb in a few plumes; Fig. 1). Here, PAL is used for evaluating the capacity of our transport model CHIMERE (see Sect. 2.2) to reproduce the methane mole fraction variability at high latitudes and at synoptic scales in a basic scenario (see Sect. 2.3). The methane mole fractions at the observation sites are analysed with instruments maintained by Environment Canada (EC, ALT), NOAA/Earth System Research Laboratory (NOAA/ESRL, BRW), and the Finnish Meteorological Institute (FMI, PAL and TIK). They are calibrated with standards traceable to the WMO X2004 CH<sub>4</sub> mole fraction scale (Dlugokencky et al., 2005). The combined standard uncertainty on individual measurement remains below the ±3.7 ppb requested by the World Meteorological Organization (WMO/GAW, 2009). Hereafter, only afternoon averages of observed mole fractions are compared to simulated equivalents to reduce the influence of very local emissions not well reproduced in the meso-scale transport model.

For enhancing atmospheric insights on ESAS emissions, we complete the statistical analysis of methane mole fractions with isotope measurements from Zeppelin observatory (ZEP) with clear identified origin from East Siberia (Fisher et al., 2011). Isotopes measurements of  $\delta^{13}\text{C}_{\text{CH}_4}$  at ZEP are carried out by the Royal Holloway University of London (RHUL). 5 L tedlar bags are collected and analysed with modified gas chromatography isotope ratio mass spectrometry (GC-IRMS) at RHUL (Fisher et al., 2011). CH<sub>4</sub> emissions from the Arctic ocean are expected to dominantly come from ESAS thawing permafrost as suggested by Shakhova et al. (2010), and less from hydrate methane destabilization. Isotopic compositions measured at ZEP during Septem-

ber 2008 and September–October 2009 (see Fig. 3) are compared to CHIMERE simulations in Sect. 3.1 for assessing methane emission processes in ESAS. No continuous observations of CH<sub>4</sub> mole fractions are carried out in 2010 to complete the statistical analysis on the 4 other selected sites.

## 2.2 Polar CHIMERE transport model

Atmospheric transport is simulated with the Eulerian meso-scale non-hydrostatic chemistry transport model CHIMERE (Vautard et al., 2001; Menut et al., 2013). The model is constrained by meteorological fields interpolated at a spatial resolution of 0.5° × 0.5° every 3 h from re-analyses of the European Centre for Medium-range Weather Forecasts (ECMWF, ERA-INTERIM; Uppala et al., 2005). The original model has been modified to simulate atmospheric transport over polar regions with a regular kilometric resolution of 35 km × 35 km covering all latitudes from 50° N up to the North Pole (see Fig. 1). Such a kilometric resolution avoids the numerical issues in grid cells becoming very small close to the pole, as it is the case for longitude/latitude regular grids. The transport simulations represent the troposphere in the region from the surface to 300 hPa (~ 9000 m) with geometrically spaced vertical layers of 10 m close to the surface and 300 m in the upper troposphere. The oxidation of CH<sub>4</sub> by the OH radicals is not considered here since the focus is put on synoptic variations of atmospheric methane mole fractions at the surface.

## 2.3 Transport inputs and emission scenarios

The regional transport model CHIMERE requires boundary mole fractions and surface emissions to simulate methane mole fractions in its limited domain. Boundary mole fractions are interpolated from global analyses obtained by assimilating surface mole fraction measurements (Locatelli et al., 2014). The 3 hourly global analyses at 3.75° × 1.875° of resolution are interpolated at the sides of CHIMERE domain for the required dates.

## Methane releases from Arctic shelves

A. Berchet et al.

Title Page

Abstract

Introduction

Conclusions

References

Tables

Figures



Back

Close

Full Screen / Esc

Printer-friendly Version

Interactive Discussion



**Methane releases  
from Arctic shelves**

A. Berchet et al.

Title Page

Abstract

Introduction

Conclusions

References

Tables

Figures



Back

Close

Full Screen / Esc

Printer-friendly Version

Interactive Discussion



Surface emissions for the CHIMERE domain are deduced from state-of-the-art models and inventories: (1) EDGAR v4.2 FT2010 inventory for year 2010 for anthropogenic emissions (<http://edgar.jrc.ec.europa.eu>), (2) LPJ model for a global monthly climatology of wetland emissions (Spahni et al., 2011), (3) GFED v3 model at a daily scale for fire emissions (Giglio et al., 2009; van der Werf et al., 2010), and (4) emissions from ESAS (see below and location in Fig. 1). The EDGAR inventory uses up-to-date economic activity maps by sector, convolved with emission factors estimated in laboratories or with statistical studies (Olivier et al., 2005). LPJ model includes a dynamical simulation of inundated wetland areas (Stocker et al., 2014), dynamic nitrogen cycle (Stocker et al., 2013), and dynamic evolution of peatlands (Spahni et al., 2013; Stocker et al., 2014). The model uses CRU TS 3.21 input data (temperature, precipitation rate, cloud cover, wet days), observed atmospheric CO<sub>2</sub> and prescribed nitrogen deposition (Lamarque et al., 2011) for each year for the simulation of dynamic forest and peatland vegetation growth. The GFED v3 database is built from the 500 m Collection 5.1 MODIS DB burned-area mapping algorithm (Giglio et al., 2009). CH<sub>4</sub> emissions at monthly and daily scales are deduced from the burnt areas using Carnegie–Ames–Stanford–Approach (CASA model; Potter et al., 1993) and emission factors (van der Werf et al., 2010).

The first three types of emissions are projected from their original grids of 0.1° × 0.1° (EDGAR) and 0.5° × 0.5° (LPJ, GFED) to CHIMERE grid. ESAS emissions are directly built on CHIMERE grid from Shakhova et al. (2010) as they provide a detailed description of the emission zones and emission strengths per period (winter/summer). As it is suggested in Shakhova et al. (2010), hot spots are separated from background emissions and summer fluxes (mid-June to mid-September) from winter ones (the rest of the year). We prescribe uniform and constant emissions by emission type (hot spots and background) and period (summer and winter). Doing so, we underestimate the variability of methane emissions from ESAS which likely vary on shorter time scales, especially in winter in relation with sea ice breaks and ice displacements after periods of accumulation under the ice. This means that simulated mole fractions are less

contrasted with smaller peaks and higher background values than with a more realistic (but unknown) flux map. We scale ESAS emissions, so that annual emissions are  $8 \text{ TgCH}_4 \text{ y}^{-1}$ .

The four types of emissions are run as separate passive tracers in polar CHIMERE for 2012, which allows analysing the contribution of each source separately at observation sites. The combination of the contributions from the four types of emissions and from the transported boundary mole fractions provides the modelled methane mole fractions including the ESAS contribution. The emission scenario not including (resp. including) ESAS emissions is hereafter called the basic (resp. reference) scenario. The basic and reference scenarios are compared to observed time series in Sect. 3.2.

## 2.4 Statistical assessment of ESAS emissions

A best guess for ESAS emission magnitude can be derived by summing scaled ESAS emissions to the basic scenario (see Sect. 2.3), so that simulated time series fit the best to observed time series (see Eq. (1) below for agreement score definition). However, the emission databases used in the transport model, as much as the lateral boundary conditions and the transport representation itself, suffer from uncertainties. A tolerance interval for ESAS emission magnitude as seen by atmospheric sites is computed through a Monte Carlo experiment to account for these uncertainties.

The Monte Carlo ensemble (20 000 samples hereafter) is generated by randomly scaling for every month of the year the anthropogenic emissions, the wetland emissions and the boundary conditions. The distributions used for these perturbations are Gaussian distributions of respectively 50, 75 and 50 % of errors. In addition to the emission scaling, we also add a random Gaussian noise on the simulated mixing ratios of 60 ppb of standard deviation. This noise on the simulations is expected to represent the errors on the transport and from the imperfect distribution of the emissions. The Monte Carlo perturbations have been chosen in the upper range of known uncertainties in the used data sets (e.g., Kirschke et al., 2013 for emissions and Patra et al., 2011 for transport), so that the final uncertainties on ESAS emissions are not under-estimated.

Methane releases  
from Arctic shelves

A. Berchet et al.

Title Page

Abstract

Introduction

Conclusions

References

Tables

Figures

◀

▶

◀

▶

Back

Close

Full Screen / Esc

Printer-friendly Version

Interactive Discussion



For every Monte Carlo sample  $i$  (i.e. a specific perturbed set of anthropogenic emissions, wetland ones, and boundary conditions, with added transport noise), model-observations agreement scores  $S$  are computed for ESAS emissions from 0 to  $20 \text{ TgCH}_4 \text{ y}^{-1}$ ; other emission rates (wetlands and anthropogenic) are not changed.

The model-observations agreement score  $S$  is the sum of the local scores  $s$  at ALT, TIK and PAL (BRW is not used in the computation of the score  $S$  as no observations are available between June and December 2012; Fig. 4). Local scores  $s$  are defined by the centered RMS distance (i.e. the distance to the reference observation point in a Taylor diagram; Taylor, 2001):

$$s^2 = 1 + \left( \frac{\sigma_s}{\sigma_o} \right)^2 - 2 \frac{\sigma_s}{\sigma_o} r \quad (1)$$

where  $\sigma_s$  (resp.  $\sigma_o$ ) is the simulated (resp. observed) standard deviation and  $r$  the correlation coefficient between the observations and the simulations at the selected site.

This statistical analysis is not performed on the whole available dataset, but on afternoon averaged mixing ratios. This processing protocol is widely used in atmospheric quantitative studies and reduces the impact of local emissions not-well mixed in the meso-scale transport model.

Tolerance intervals  $\text{TI}_i$  for ESAS emissions are deduced for all samples of the Monte Carlo ensemble, so that all ESAS emissions with associated scores within  $[S_{\min}, S_{\min} + 10\%]$  are considered compatible with the atmospheric signal, with  $S_{\min}$  is the minimum agreement score for the Monte Carlo sample  $i$ . These tolerance intervals are computed for every month of the year 2010. In the end, for every month of the year 2010, we compute aggregated tolerance intervals for ESAS methane emissions such that 95% (equivalent to  $2\sigma$  interval for Gaussian distributions) of the Monte Carlo ensemble is within the interval.

### 3 Results

In the following, isotopic remote observations are used to confirm the origin of ESAS methane, simulated mole fractions for the four contributions mentioned above are compared with methane observations and analysed using the Monte Carlo statistical analysis described in Sect. 2.4 to estimate the methane emissions from the ESAS which best fit the atmospheric methane observations.

#### 3.1 Summer isotopic observations in the Arctic

To confirm the assertion that ESAS thawing permafrost dominates Arctic ocean emissions and to bring qualitative information on the relative contribution of each emission process in the Arctic, we analyse isotopic composition of Arctic air ( $\delta^{13}\text{C}_{\text{CH}_4}$  here), as measured at ZEP observatory in September 2008 and September–October 2009. Arctic surface emissions mixed into the atmosphere own very different isotopic signatures: typically of  $-40/ -55\text{‰}$  for gas leaks,  $-50/ -55\text{‰}$  for marine hydrates and  $-60/ -75\text{‰}$  for wetlands and permafrost thawing (Fisher et al., 2011; Milkov, 2005). During the observation campaigns, episodes at ZEP with identified origin from River Ob and Eastern Siberia exhibited a mean signature of  $-65 \pm 3\text{‰}$  in September 2008 (Fisher et al., 2011) and of  $-68 \pm 5\text{‰}$  in 2009 (see Fig. 3). In these air masses, with Shakhova et al. (2010) scenario transported by CHIMERE, ESAS emissions contribute to 40–50 % of the signal at ZEP and continental wetlands (resp. fossil fuels) to 35 % (resp. 20 %). Using these relative weights to estimate the integrated isotopic signature at ZEP, ESAS emissions from marine hydrates would imply a simulated  $\delta^{13}\text{C}_{\text{CH}_4}$  of  $-51/ -61\text{‰}$ , thus not compatible with the observations.

As ZEP isotopic observations give integrated constraints on  $\text{CH}_4$  emissions from ESAS as a whole, significant methane emissions from ESAS are only compatible with isotopic observations if mainly originating from microbial processes, which is consistent with Shakhova et al. (2010) conclusions based on their in-situ measurements.

## Methane releases from Arctic shelves

A. Berchet et al.

Title Page

Abstract

Introduction

Conclusions

References

Tables

Figures



Back

Close

Full Screen / Esc

Printer-friendly Version

Interactive Discussion



## 3.2 Model–observation comparisons at four Arctic sites

At PAL, BRW and ALT, the continuous methane observations exhibit similar seasonal variations with a minimum during summer (June–July) and a maximum during winter (December–January). At PAL and less evidently at ALT, the synoptic variations appear larger in winter than in summer. At TIK, the seasonal maximum is observed in August, associated with large synoptic variations and a less pronounced seasonal cycle, suggesting an influence of local to regional emissions during summer months.

At PAL, a site scarcely influenced by ESAS emissions, most of the atmospheric signal is explained by boundary conditions, especially the large synoptic variations during winter months. Polar-CHIMERE computed with our basic emission scenario demonstrates a very good (resp. good) skill in winter (resp. summer) in representing the atmospheric methane mole fraction variability at high latitude sites. As shown in Fig. 4A, the variability of the daily averages observed methane mole fractions is indeed well captured by CHIMERE (annual temporal correlation of  $r = 0.87$ ; winter  $r = 0.89$ ; summer  $r = 0.63$ ; Tab. 1). Discrepancies between the observed signal and the simulated one at other sites can then be reasonably interpreted in terms of mis-specified regional emissions.

At ALT and BRW (Fig. 4b and c), two sites remote from ESAS but influenced by long-range transport from ESAS across the Arctic ocean (see Figs. S7 and S8), winter mole fractions (i.e. the year outside June–September) are well reproduced by the basic scenario ( $r = 0.79$  and  $r = 0.76$ , respectively). In the reference scenario (see Sect. 2.3), the contribution of ESAS is much too large at ALT and BRW in winter as shown by the large blue spikes of Fig. 4 between January and April and between October to December (ALT only, no data available for BRW during summer 2012). Moreover, as discussed in Sect. 2.3, the time distribution of ESAS emissions is not represented. A realistic time distribution would have led to enhanced simulated spikes, reinforcing the inconsistency of winter ESAS fluxes.

### Methane releases from Arctic shelves

A. Berchet et al.

Title Page

Abstract

Introduction

Conclusions

References

Tables

Figures



Back

Close

Full Screen / Esc

Printer-friendly Version

Interactive Discussion



**Methane releases  
from Arctic shelves**

A. Berchet et al.

Title Page

Abstract

Introduction

Conclusions

References

Tables

Figures



Back

Close

Full Screen / Esc

Printer-friendly Version

Interactive Discussion



In summer, at ALT, the fit of the reference scenario to the observations is less favourable than in winter ( $r = 0.56$ ). Adding ESAS emissions may fill some gaps in July–August, less in June and September, though some spikes are too high and phases are not always in agreement with observations. Some summer peaks from the ESAS are very well reproduced by the model (Fig. 4) at ALT in July/August. This would suggest that sudden bursts of methane may be released on short periods (typically days) during July and August, with instantaneous rates corresponding to  $8 \text{ TgCH}_4 \text{ y}^{-1}$ , but not on the long run.

Getting closer to the ESAS, TIK methane observations compared to simulations confirm that the simulated contribution of ESAS emissions from January to April and from October to December is over-estimated (Fig. 4d). Indeed, the baseline of observations is well reproduced by the basic scenario, despite some unexplained spikes in winter (Fig. 4d), which slightly decorrelate the fit of the basic scenario to observations ( $r = 0.56$ , Tab. 1). These spikes can be attributed either to small and short-term releases of  $\text{CH}_4$  from ESAS or to other emissions not properly represented or transported to TIK. In June, the contribution from the ESAS is still too large compared to observations. However, from July to September, the observed mole fractions are higher and more variable than the basic scenario. This suggest emissions from ESAS that are compatible with the  $8 \text{ TgCH}_4 \text{ y}^{-1}$  scenario, or even higher, for these 3 months.

Indeed, as confirmed by the footprint analysis at TIK (supplementary material; Fig. S6), observations from July to September are mostly influenced by regional emissions (closer than 200 km), including ESAS. However, within this radius of influence, wetland emissions from north Yakutia (mainly along Laptev sea shores between Lena and Indigirka rivers) could also significantly contribute to methane mole fractions at TIK. If such wetlands are ill-represented in LPJ model at  $0.5^\circ$  of resolution (either in magnitude or timing), this could dampen the compatibility of the  $8 \text{ TgCH}_4 \text{ y}^{-1}$  scenario with TIK observations for summer months.

In summary, the emission scenario from Shakhova et al. (2010) shows a large over-estimation of methane mole fractions at Arctic stations during all months but from July



## Methane releases from Arctic shelves

A. Berchet et al.

Title Page

Abstract

Introduction

Conclusions

References

Tables

Figures

◀

▶

◀

▶

Back

Close

Full Screen / Esc

Printer-friendly Version

Interactive Discussion



This estimate is an upper bound for ESAS emissions for the two following reasons. First, the monthly flat temporal emission profile from ESAS in our emission scenario underestimates the impact of ESAS region on synoptic methane variations at observation sites. In the real world, concentration peaks due to shorter and more intense methane release from ESAS would be larger, thus reducing further the estimated emissions in order to match atmospheric observations. Second, though wetland emissions has been perturbed in the Monte Carlo sensitivity analysis, this perturbation has been carried out with a centered Gaussian distribution, whereas the local and regional influence of wetlands may be systematically under-estimated in the global LPJ model. The most extensive wetland area (a 200–300 km wide coastal lowland) in the vicinity of TIK is located to the East. Wetland emissions from this area may be either missing or partly displaced in a global model such as LPJ. More work is needed to provide a more realistic regional wetland scenario, but such unaccounted or underestimated wetland emissions could reduce our ESAS emission estimates (in order to match the observed concentration at TIK).

## 4 Conclusions

We suggest some insights on Eastern Siberian Arctic Shelf CH<sub>4</sub> emissions using atmospheric methane observations, to complete the intensive in-situ measurement campaigns carried out mostly in summer in the region. We test the consistency of a methane emission scenario including a 8 TgCH<sub>4</sub>y<sup>-1</sup> source from the ESAS. This scenario is run in a high-resolution model representing Arctic atmospheric transport and confronted to continuous methane concentrations performed at remote and nearby continuous atmospheric stations.  $\delta^{13}\text{C}_{\text{CH}_4}$  observations are also used to identify the dominant process emitting methane. The analysis of the modelled and observed time series suggests a large overestimation of ESAS emissions in winter, but still a high contribution of ESAS emissions from July and August, also consistent with isotopic observations. Over 2012, a statistical analysis based on model/observations comparison

**Methane releases  
from Arctic shelves**

A. Berchet et al.

Title Page

Abstract

Introduction

Conclusions

References

Tables

Figures



Back

Close

Full Screen / Esc

Printer-friendly Version

Interactive Discussion



is performed to estimate ESAS emissions and address the uncertainties of our approach. Our method suggests emissions from ESAS of 0.5 to 4.3 Tg CH<sub>4</sub> y<sup>-1</sup>. Although significant at the regional scale, especially in summer, these revised emissions are about 2 to 5 times smaller than previous estimates from Shakhova et al. (2010) and 6 to 10 times smaller than the most recent estimates (Shakhova et al., 2014). The time series from the different sites also confirm a very likely heterogeneous temporal variability and spatial distribution, with very short and local methane releases from ESAS. A multi-year analysis with more observation sites and an improved representation of the regional wetland should be carried out in order to reduce the uncertainties in ESAS emission estimates and to properly identify the sensitivity of the emissions to the ice cover or to other meteorological conditions and the distribution and short-scale variability of the fluxes. The use of another transport model would also be important to address biases in the representation of transport, not addressed by our statistical analysis based on centered perturbations. The development of continuous <sup>13</sup>CH<sub>4</sub> observations at Arctic observation sites, now possible through cavity ring down spectrometry, would provide additional constraints for partitioning emissions between marine hydrates, gas leaks, thawing permafrost and continental wetlands. Finally, the observatories operated around the Arctic Ocean could also provide more quantitative estimates of Arctic emissions from ESAS using direct and inverse modelling of both CH<sub>4</sub> and <sup>13</sup>CH<sub>4</sub> observations.

**The Supplement related to this article is available online at  
doi:10.5194/acpd-15-25477-2015-supplement.**

*Acknowledgements.* We thank the PI from the observation sites we used for maintaining methane measurements at high latitudes and sharing their data. We also thank F. Marabelle (LSCE) and the LSCE IT team for the computer resources. This study was supported by the CEA, ANR-CLIMSLIP project and iZomet Franco–Swedish project.

## References

- Bousquet, P., Ringeval, B., Pison, I., Dlugokencky, E. J., Brunke, E.-G., Carouge, C., Chevalier, F., Fortems-Cheiney, A., Frankenberg, C., Hauglustaine, D. A., Krummel, P. B., Langenfelds, R. L., Ramonet, M., Schmidt, M., Steele, L. P., Szopa, S., Yver, C., Viovy, N., and Ciais, P.: Source attribution of the changes in atmospheric methane for 2006–2008, *Atmos. Chem. Phys.*, 11, 3689–3700, doi:10.5194/acp-11-3689-2011, 2011. 25479
- Collins, M., Knutti, R., Arblaster, J., Dufresne, J., Fichet, T., Friedlingstein, P., Gao, X., Gutowski, W., Johns, T., Krinner, G., Shongwe, M., Tebaldi, C., Weaver, A., and Wehner, M.: Long-term climate change: projections, commitments and irreversibility, in: *Climate Change 2013: The Physical Science Basis. Contribution of Working Group I to the Fifth Assessment Report of the Intergovernmental Panel on Climate Change*, edited by: Stocker, T., Qin, D., Plattner, G., Tignor, M., Allen, S., Boschung, J., Nauels, A., Xia, Y., Bex, V., and Midgley, P., Cambridge University Press, Cambridge, UK, 2013. 25478
- Dlugokencky, E. J., Steele, L. P., Lang, P. M., and Masarie, K. A.: Atmospheric methane at Mauna Loa and Barrow observatories: presentation and analysis of in situ measurements, *J. Geophys. Res.-Atmos.*, 100, 23103–23113, doi:10.1029/95JD02460, 1995. 25496
- Dlugokencky, E. J., Myers, R. C., Lang, P. M., Masarie, K. A., Crotwell, A. M., Thoning, K. W., Hall, B. D., Elkins, J. W., and Steele, L. P.: Conversion of NOAA atmospheric dry air CH<sub>4</sub> mole fractions to a gravimetrically prepared standard scale *J. Geophys. Res.*, 110, D18306, doi:10.1029/2005JD006035, 2005. 25481
- Dlugokencky, E. J., Crotwell, A. M., Lang, P. M., and Masarie, K. A.: Atmospheric methane dry air mole fractions from quasi-continuous measurements at Barrow, Alaska and Mauna Loa, Hawaii, 1986–2013, available at: [ftp://aftp.cmdl.noaa.gov/data/trace\\_gases/ch4/in-situ](ftp://aftp.cmdl.noaa.gov/data/trace_gases/ch4/in-situ) (last access: 15 September 2015), 2014. 25496
- Fisher, R. E., Srisankantharajah, S., Lowry, D., Lanoisellé, M., Fowler, C. M. R., James, R. H., Hermansen, O., Lund Myhre, C., Stohl, A., Greinert, J., Nisbet-Jones, P. B. R., Mienert, J., and Nisbet, E. G.: Arctic methane sources: isotopic evidence for atmospheric inputs, *Geophys. Res. Lett.*, 38, L21803, doi:10.1029/2011GL049319, 2011. 25479, 25481, 25486, 25496
- Giglio, L., Loboda, T., Roy, D. P., Quayle, B., and Justice, C. O.: An active-fire based burned area mapping algorithm for the MODIS sensor, *Remote Sens. Environ.*, 113, 408–420, doi:10.1016/j.rse.2008.10.006, 2009. 25483

**Methane releases  
from Arctic shelves**

A. Berchet et al.

Title Page

Abstract

Introduction

Conclusions

References

Tables

Figures



Back

Close

Full Screen / Esc

Printer-friendly Version

Interactive Discussion



- Kirschke, S., Bousquet, P., Ciais, P., Saunio, M., Canadell, J. G., Dlugokencky, E. J., Bergamaschi, P., Bergmann, D., Blake, D. R., Bruhwiler, L., Cameron-Smith, P., Castaldi, S., Chevallier, F., Feng, L., Fraser, A., Heimann, M., Hodson, E. L., Houweling, S., Josse, B., Fraser, P. J., Krummel, P. B., Lamarque, J.-F., Langenfelds, R. L., Le Quéré, C., Naik, V., O'Doherty, S., Palmer, P. I., Pison, I., Plummer, D., Poulter, B., Prinn, R. G., Rigby, M., Ringeval, B., Santini, M., Schmidt, M., Shindell, D. T., Simpson, I. J., Spahni, R., Steele, L. P., Strode, S. A., Sudo, K., Szopa, S., van der Werf, G. R., Voulgarakis, A., van Weele, M., Weiss, R. F., Williams, J. E., and Zeng, G.: Three decades of global methane sources and sinks, *Nat. Geosci.*, 6, 813–823, doi:10.1038/ngeo1955, 2013. 25479, 25484
- Lamarque, J.-F., Kyle, G. P., Meinshausen, M., Riahi, K., Smith, S. J., Vuuren, D. P. v., Conley, A. J., and Vitt, F.: Global and regional evolution of short-lived radiatively-active gases and aerosols in the representative concentration pathways, *Climatic Change*, 109, 191–212, doi:10.1007/s10584-011-0155-0, 2011. 25483
- Locatelli, R., Bousquet, P., Hourdin, F., Saunio, M., Cozic, A., Couvreux, F., Grandpeix, J.-Y., Lefebvre, M.-P., Rio, C., Bergamaschi, P., Chambers, S. D., Karstens, U., Kazan, V., van der Laan, S., Meijer, H. A. J., Moncrieff, J., Ramonet, M., Scheeren, H. A., Schlosser, C., Schmidt, M., Vermeulen, A., and Williams, A. G.: Atmospheric transport and chemistry of trace gases in LMDz5B: evaluation and implications for inverse modelling, *Geosci. Model Dev.*, 8, 129–150, doi:10.5194/gmd-8-129-2015, 2015. 25482
- McGuire, A. D., Anderson, L. G., Christensen, T. R., Dallimore, S., Guo, L., Hayes, D. J., Heimann, M., Lorenson, T. D., Macdonald, R. W., and Roulet, N.: Sensitivity of the carbon cycle in the Arctic to climate change, *Ecol. Monogr.*, 79, 523–555, doi:10.1890/08-2025.1, 2009. 25479
- Menut, L., Bessagnet, B., Khvorostyanov, D., Beekmann, M., Blond, N., Colette, A., Coll, I., Curci, G., Foret, G., Hodzic, A., Mailler, S., Meleux, F., Monge, J.-L., Pison, I., Siour, G., Turquety, S., Valari, M., Vautard, R., and Vivanco, M. G.: CHIMERE 2013: a model for regional atmospheric composition modelling, *Geosci. Model Dev.*, 6, 981–1028, doi:10.5194/gmd-6-981-2013, 2013. 25482
- Milkov, A. V.: Molecular and stable isotope compositions of natural gas hydrates: a revised global dataset and basic interpretations in the context of geological settings, *Org. Geochem.*, 36, 681–702, doi:10.1016/j.orggeochem.2005.01.010, 2005. 25486
- Olivier, J. G. J., Van Aardenne, J. A., Dentener, F. J., Pagliari, V., Ganzeveld, L. N., and Peters, J. A. H. W.: Recent trends in global greenhouse gas emissions: regional trends

**Methane releases  
from Arctic shelves**

A. Berchet et al.

Title Page

Abstract

Introduction

Conclusions

References

Tables

Figures



Back

Close

Full Screen / Esc

Printer-friendly Version

Interactive Discussion



1970–2000 and spatial distribution of key sources in 2000, *Environm. Sci.*, 2, 81–99, doi:10.1080/15693430500400345, 2005. 25483

Patra, P. K., Houweling, S., Krol, M., Bousquet, P., Belikov, D., Bergmann, D., Bian, H., Cameron-Smith, P., Chipperfield, M. P., Corbin, K., Fortems-Cheiney, A., Fraser, A., Gloor, E., Hess, P., Ito, A., Kawa, S. R., Law, R. M., Loh, Z., Maksyutov, S., Meng, L., Palmer, P. I., Prinn, R. G., Rigby, M., Saito, R., and Wilson, C.: TransCom model simulations of CH<sub>4</sub> and related species: linking transport, surface flux and chemical loss with CH<sub>4</sub> variability in the troposphere and lower stratosphere, *Atmos. Chem. Phys.*, 11, 12813–12837, doi:10.5194/acp-11-12813-2011, 2011. 25484

Potter, C. S., Randerson, J. T., Field, C. B., Matson, P. A., Vitousek, P. M., Mooney, H. A., and Klooster, S. A.: Terrestrial ecosystem production: a process model based on global satellite and surface data, *Global Biogeochem. Cy.*, 7, 811–841, doi:10.1029/93GB02725, 1993. 25483

Sasakawa, M., Shimoyama, K., Machida, T., Tsuda, N., Suto, H., Arshinov, M., Davydov, D., Fofonov, A., Krasnov, O., Saeki, T., Koyama, Y., and Maksyutov, S.: Continuous measurements of methane from a tower network over Siberia, *Tellus B*, 62, 403–416, doi:10.1111/j.1600-0889.2010.00494.x, 2010. 25480

Shakhova, N., Semiletov, I., Salyuk, A., Yusupov, V., Kosmach, D., and Gustafsson, O.: Extensive methane venting to the atmosphere from sediments of the East Siberian Arctic Shelf, *Science*, 327, 1246–1250, doi:10.1126/science.1182221, 2010. 25479, 25480, 25481, 25483, 25486, 25488, 25489, 25491, 25501

Shakhova, N., Semiletov, I., Leifer, I., Sergienko, V., Salyuk, A., Kosmach, D., Chernykh, D., Stubbs, C., Nicolosky, D., Tumskey, V., and Gustafsson, R.: Ebullition and storm-induced methane release from the East Siberian Arctic Shelf, *Nat. Geosci.*, 7, 64–70, doi:10.1038/ngeo2007, 2014. 25479, 25480, 25491

Spahni, R., Wania, R., Neef, L., van Weele, M., Pison, I., Bousquet, P., Frankenberg, C., Foster, P. N., Joos, F., Prentice, I. C., and van Velthoven, P.: Constraining global methane emissions and uptake by ecosystems, *Biogeosciences*, 8, 1643–1665, doi:10.5194/bg-8-1643-2011, 2011. 25483

Spahni, R., Joos, F., Stocker, B. D., Steinacher, M., and Yu, Z. C.: Transient simulations of the carbon and nitrogen dynamics in northern peatlands: from the Last Glacial Maximum to the 21st century, *Clim. Past*, 9, 1287–1308, doi:10.5194/cp-9-1287-2013, 2013. 25483

## Methane releases from Arctic shelves

A. Berchet et al.

Title Page

Abstract

Introduction

Conclusions

References

Tables

Figures



Back

Close

Full Screen / Esc

Printer-friendly Version

Interactive Discussion



Stocker, B. D., Roth, R., Joos, F., Spahni, R., Steinacher, M., Zaehle, S., Bouwman, L., Xu-Ri, and Prentice, I. C.: Multiple greenhouse-gas feedbacks from the land biosphere under future climate change scenarios, *Nature Clim. Change*, 3, 666–672, doi:10.1038/nclimate1864, 2013. 25483

5 Stocker, B. D., Spahni, R., and Joos, F.: DYPTOP: a cost-efficient TOPMODEL implementation to simulate sub-grid spatio-temporal dynamics of global wetlands and peatlands, *Geosci. Model Dev.*, 7, 3089–3110, doi:10.5194/gmd-7-3089-2014, 2014. 25483

Taylor, K. E.: Summarizing multiple aspects of model performance in a single diagram, *J. Geophys. Res.-Atmos.*, 106, 7183–7192, doi:10.1029/2000JD900719, 2001. 25485

10 Uppala, S. M., Kållberg, P. W., Simmons, A. J., Andrae, U., Bechtold, V. D. C., Fiorino, M., Gibson, J. K., Haseler, J., Hernandez, A., Kelly, G. A., Li, X., Onogi, K., Saarinen, S., Sokka, N., Allan, R. P., Andersson, E., Arpe, K., Balmaseda, M. A., Beljaars, A. C. M., Berg, L. V. D., Bidlot, J., Bormann, N., Caires, S., Chevallier, F., Dethof, A., Dragosavac, M., Fisher, M., Fuentes, M., Hagemann, S., Hólm, E., Hoskins, B. J., Isaksen, I., Janssen, P. A. E. M., Jenne, R., McNally, A. P., Mahfouf, J.-F., Morcrette, J.-J., Rayner, N. A., Saunders, R. W., Simon, P., Sterl, A., Trenberth, K. E., Untch, A., Vasiljevic, D., Viterbo, P., and Woollen, J.: The ERA-40 re-analysis, *Q. J. Roy. Meteor. Soc.*, 131, 2961–3012, doi:10.1256/qj.04.176, 2005. 25482

20 van der Werf, G. R., Randerson, J. T., Giglio, L., Collatz, G. J., Mu, M., Kasibhatla, P. S., Morton, D. C., DeFries, R. S., Jin, Y., and van Leeuwen, T. T.: Global fire emissions and the contribution of deforestation, savanna, forest, agricultural, and peat fires (1997–2009), *Atmos. Chem. Phys.*, 10, 11707–11735, doi:10.5194/acp-10-11707-2010, 2010. 25483

Vautard, R., Beekmann, M., Roux, J., and Gombert, D.: Validation of a hybrid forecasting system for the ozone concentrations over the Paris area, *Atmos. Environ.*, 35, 2449–2461, doi:10.1016/S1352-2310(00)00466-0, 2001. 25482

25 WMO/GAW: Guidelines for the Measurement of Methane and Nitrous Oxide and their Quality Assurance (WMO/TD-No. 1478), Tech. Rep. 185, World Meteorological Organization Global Atmospheric Watch, Geneva, Switzerland, available at: [http://www.wmo.int/pages/prog/arep/gaw/documents/Final\\_GAW\\_206\\_web.pdf](http://www.wmo.int/pages/prog/arep/gaw/documents/Final_GAW_206_web.pdf) (last access: 15 September 2015), 2009. 25481

Methane releases  
from Arctic shelves

A. Berchet et al.

Title Page

Abstract

Introduction

Conclusions

References

Tables

Figures

I◀

▶I

◀

▶

Back

Close

Full Screen / Esc

Printer-friendly Version

Interactive Discussion

**Table 1.** Observation site characteristics. The site location is displayed in Fig. 1.

Station	ID	Location			Network/ Institute (data server)	Reference correlations $r$	
		Lon (° E)	Lat (° N)	Alt (m a.s.l.)		Winter	Summer
Alert	ALT	−62.5	82.5	200	EC (WDCCGG <sup>1</sup> )	0.79	0.56
Barrow	BRW	−156.6	71.3	11	NOAA/ESRL (ESRL <sup>2</sup> )	0.76	–
Tiksi	TIK	128.9	71.6	42	FMI (ESRL <sup>3</sup> )	0.56	−0.04
Pallas	PAL	24.12	68.0	560	FMI (WDCGG <sup>1</sup> )	0.89	0.63
Zeppelin	ZEP	11.9	79.9	475	RHUL (Fisher et al., 2011)	–	–

<sup>1</sup> World Data Center for Greenhouse Gases (<http://ds.data.jma.go.jp/gmd/wdogg/>)<sup>2</sup> Dlugokencky et al., 1995, 2014 ([ftp://aftp.cmdl.noaa.gov/data/trace\\_gases/ch4/](ftp://aftp.cmdl.noaa.gov/data/trace_gases/ch4/))<sup>3</sup> [ftp://ftp.etl.noaa.gov/psd3/arctic/tiksi/greenhouse\\_gas/ghg\\_concentration/raw/](ftp://ftp.etl.noaa.gov/psd3/arctic/tiksi/greenhouse_gas/ghg_concentration/raw/)

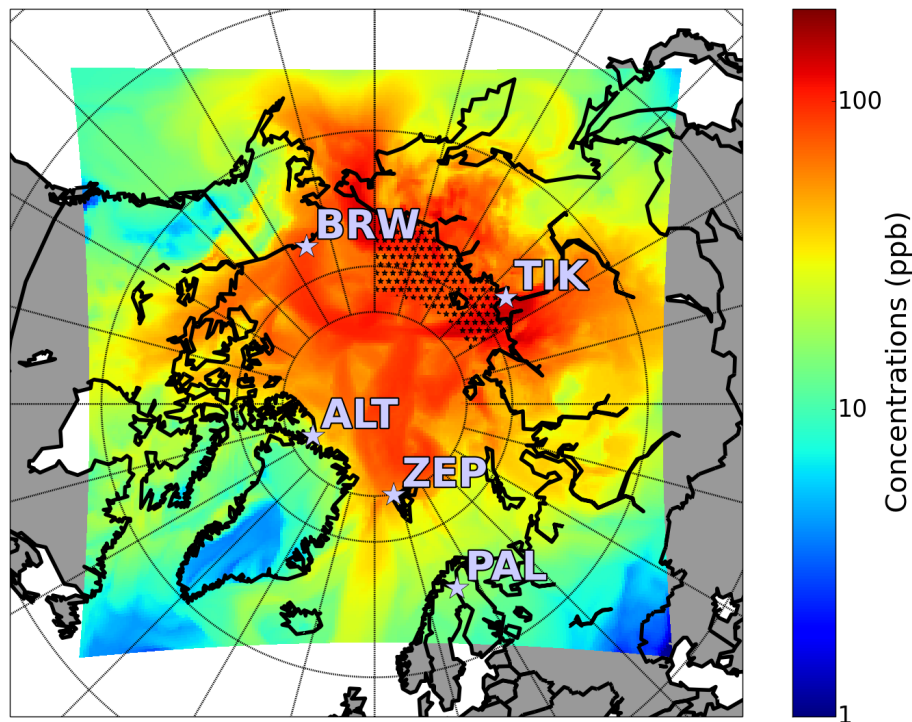


**Figure 1.** Map of the domain of CHIMERE simulations (see Sect. 2.2) with the emission zone from ESAS (black stars; see Sect. 2.3) and the stations used in the analysis. Shaded colours show the maximum over the whole year 2012 of near-surface simulated influence (in ppb) of the ESAS methane emissions after transport.

Methane releases from Arctic shelves

A. Berchet et al.

Title Page	
Abstract	Introduction
Conclusions	References
Tables	Figures
◀	▶
◀	▶
Back	Close
Full Screen / Esc	
Printer-friendly Version	
Interactive Discussion	



## Methane releases from Arctic shelves

A. Berchet et al.

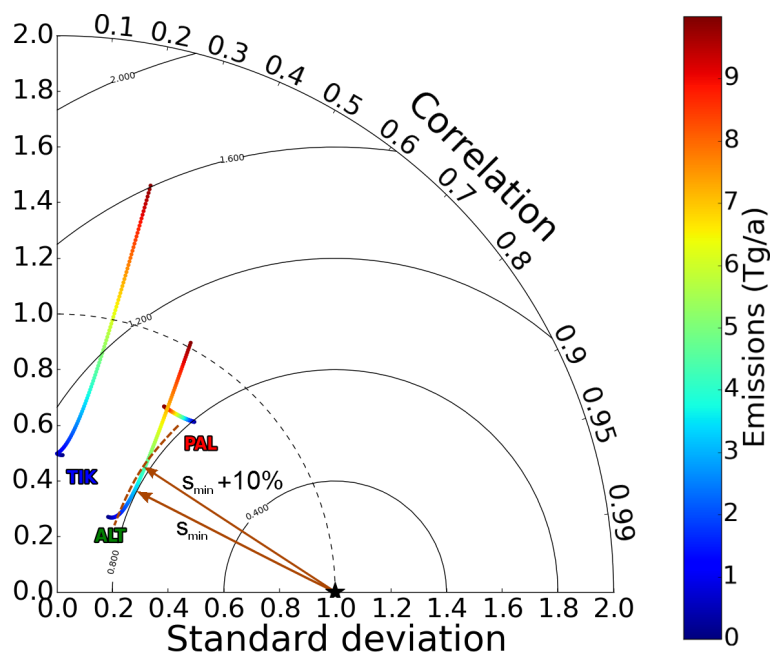


**Figure 2.** Taylor diagram representation of the statistical analysis of ESAS emissions. For each observation site, ESAS emission scenarios from 0 to  $10 \text{ TgCH}_4 \text{ y}^{-1}$  are located on the Taylor diagram, depending on the compatibility (correlation and standard deviation) between observations and simulations, thus generating a compatibility trajectory. Point colours depict the ESAS emission magnitude for each scenarios. To compare the different sites, each trajectory has been normalized by the site standard deviation. For each site, the point of the emission trajectory closest to the reference point (black star) suggests the most plausible emission rate. We compute a tolerance interval such that all ESAS emissions within  $(s_{\min}, s_{\min} + 10\%)$  are considered compatible with the atmospheric signal.

Methane releases  
from Arctic shelves

A. Berchet et al.

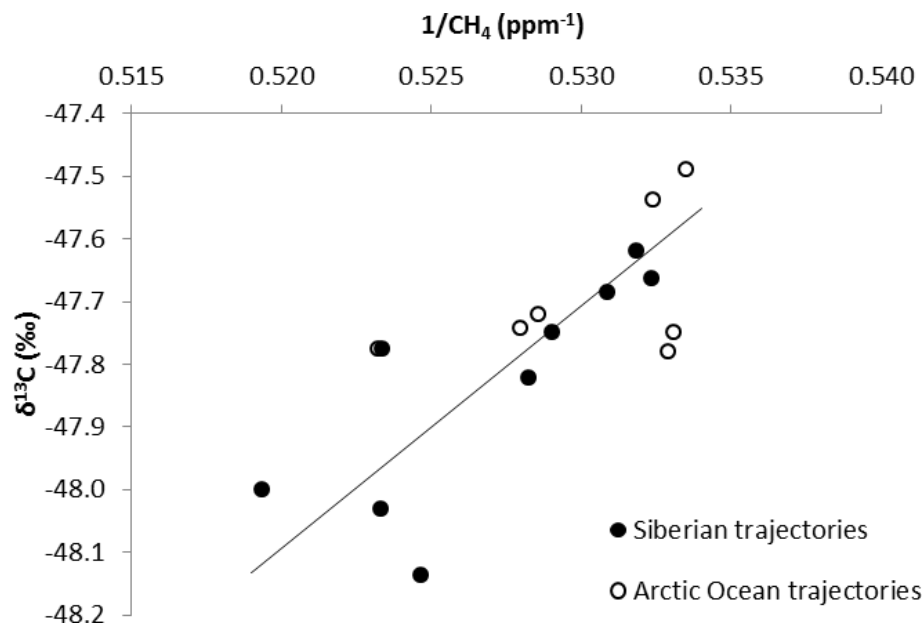


**Figure 3.** Keeling plot for observations carried out at ZEP observatory in September–October 2009. Only the observations with a dominant origin from the ESAS and Siberia or from the Arctic Ocean are kept here. The y axis intercept of the Keeling plot is  $-68 \pm 5\text{‰}$ .

Title Page

Abstract

Introduction

Conclusions

References

Tables

Figures

◀

▶

◀

▶

Back

Close

Full Screen / Esc

Printer-friendly Version

Interactive Discussion



## Methane releases from Arctic shelves

A. Berchet et al.

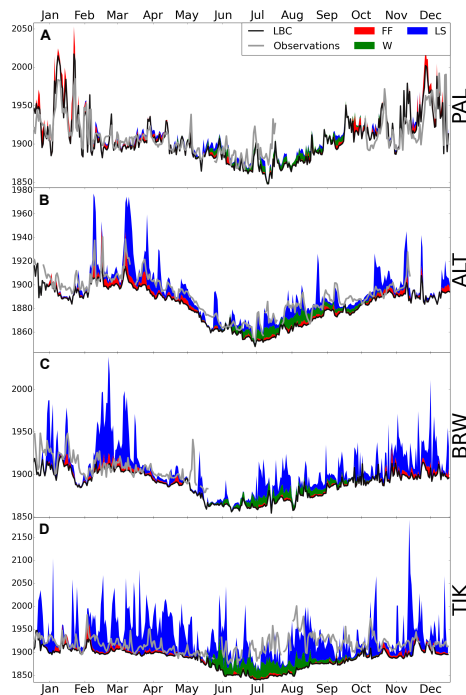


**Figure 4.** Time series of observed and simulated methane mole fractions at four Arctic sites in 2012. The filled areas depict the daily afternoon contributions from wetlands (W, green), fossil fuels and other anthropogenic emissions (FF, red) and from the ESAS (LS, blue;  $8 \text{ TgCH}_4 \text{ y}^{-1}$  scenario; Sect. 2.3). The LBC line (black) represents the contribution of the lateral boundary conditions transported into the domain. Grey lines are observations (daily averages of continuous measurements). Fire emissions are not represented in this figure due to very low influence on the studied sites.

Methane releases  
from Arctic shelves

A. Berchet et al.

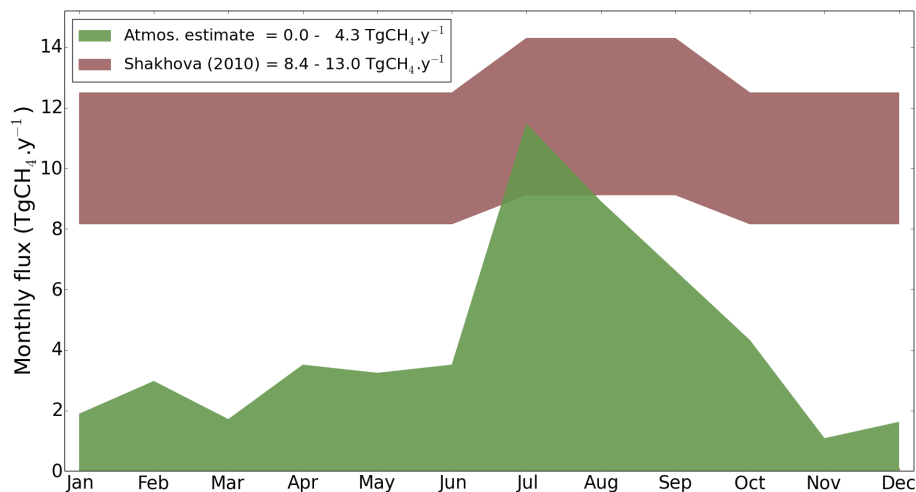


**Figure 5.** Monthly fluxes in TgCH<sub>4</sub>.y<sup>-1</sup> as deduced from agreement scores (green; see Sect. 2.4) computed for every month of the year 2012, compared to Shakhova et al. (2010) fluxes (red).